*The 2017 World Congress on*
***Advances in Structural Engineering and Mechanics (ASEM17)***
*28 August - 1 September, 2017, Ilsan(Seoul), Korea*

# Evaluation of flexural behavior of 2-span beams prestressed with unbonded high-strength strands of 2400 MPa

*Kyungmin Kim[1)], Ah Sir Cho[2)], Jun-Mo Yang[3)] and Thomas H.-K. Kang[4)]

[1),2),4)] *Department of Architecture & Architectural Engineering, Seoul National University, Seoul, Korea*
[3)] *Product Application Center, POSCO, Incheon, Korea*
[4)] tkang@snu.ac.kr

## ABSTRACT

Strands of 1860 MPa strength have been universally used for prestressing systems. Recently, high-strength strands with 2400 MPa ultimate strength were developed in Korea, and their specifications have been included in Korean Standard (KS D 7002). With this technical trend, a test program for four 2-span post-tensioned beams with unbonded high-strength strands was planned and carried out. The test specimens consisted of two 2-span beams post-tensioned with normal-strength strands and two 2-span beams post-tensioned with high-strength strands. The tendon profile was designed as one of the test variables. Through the analysis of the experimental data from four 2-span specimens under static loading up to failure, major features of flexural behavior for 2-span post-tensioned beams are investigated in this paper. Especially, evaluation procedure for estimating the tendon stress in the continuous post-tensioned beams is carried out to compare the behavior of post-tensioned beams with strands of two different strengths.

## 1. INTRODUCTION

Prestressed concrete has been used in many applications today in order to efficiently control cracking and deflection of concrete structures. Over the past half century, the use of prestressing has been significantly increased and the prestressing system is now used in wide ranges of challenging structures such as high-rise buildings, nuclear containment structures and mega-structures.

To prestress concrete members, strands with 1860 MPa of strength have been commonly used. Recently, high-strength strands with 2400 MPa ultimate strength were developed in Korea, and their specifications have been included in Korean Standard

---

[1)] Master Student
[2)] Ph.D. Student
[3)] Senior Researcher
[4)] Associate Professor

(KS D 7002). Since then, a handful of studies have been performed to examine and verify material performance of the newly developed strands (Yim 2015; Yang 2015). The studies mainly focused on the transfer length and the anchorage length of the high-strength strands in concrete members, which are major issues in pre-tensioned concrete.

Compared to the research on the behavior of high-strength strands in pre-tensioned systems, however, research on the behavior of high-strength strands in post-tensioned systems is quite limited. In order to apply high-strength strands to post-tensioned members, it is essential to verify the performance of the behavior of unbonded strands in the members. To evaluate and discuss the application of high-strength strands, a test program for four 2-span post-tensioned beams with unbonded strands was planned and carried out. The test specimens consisted of two 2-span beams with normal-strength strands and two 2-span beams with high-strength strands. The tendon profile was designed as one of the test variables.

Experimental data from four 2-span specimens under static loading are investigated in this paper. Especially, evaluation of the tendon stress in the continuous post-tensioned beams is carried out to compare the behavior of strands with two different strengths. The results in this paper lay the foundation for the future discussion on the possible revision of the current design code for practical use of 2400 MPa high-strength strands.

## 2. EXPERIMENTAL PROGRAM

### *2.1 Specimens*

Table 1 Basic parameters of test specimens

| Specimen | Strand Strength | $F_{se}$ | $f'_c$ | $f_y$ | $f_{ps}$ | $M_n$ | $\rho$, % | $\rho_p$, % | *L*/*h* | Number of Tendons |
|---|---|---|---|---|---|---|---|---|---|---|
| | MPa | kN | MPa | MPa | MPa | kN-m | | | | |
| B4H | 1860 | 622.4 | 48.0 | 478.2 | 1330.9 | 423.7 | 0.49 | 0.35 | 15.2 | 4 |
| B4L | 1860 | 622.4 | 48.0 | 478.2 | 1300.1 | 353.6 | 0.49 | 0.44 | 15.2 | 4 |
| D3H | 2400 | 613.7 | 55.0 | 478.2 | 1757.3 | 424.0 | 0.49 | 0.26 | 15.2 | 3 |
| D3L | 2400 | 613.7 | 55.0 | 478.2 | 1710.3 | 353.8 | 0.49 | 0.33 | 15.2 | 3 |

$F_{se}$ = measured effective tendon force at jacking end, $f'_c$ = measured concrete compressive strength, $f_y$ = measured yield strength of mild steel reinforcement, $f_{ps}$= stress in prestressing reinforcement at nominal flexural strength calculated based on $F_{se}$ as per ACI 318-14, $M_n$ = maximum nominal flexural strength along the length calculated based on $f_{ps}$, $\rho$ = ratio of $A_s$ to $bd_s$, $A_s$ = area of tension reinforcement, $b$ = beam width, $d_s$ = distance from extreme compression fiber to centroid of tension reinforcing bars, $\rho_p$= ratio of $A_{ps}$ to $bd_p$, $A_{ps}$ = area of prestressing reinforcement, $d_p$ = area of prestressing reinforcement, $L$ = span length, and $h$ = beam depth.

The four post-tensioned beam specimens with unbonded tendons had rectangular sections. The specimens were equal in size, but the number, type and profile of tendons were different. Detailed section properties are shown in Fig. 1. The beams were continuous over two spans, and 14.6 m in total length. The span-depth ratio of

each member was kept to be 15.2 to simulate realistic post-tensioned beam design and behavior such as flexural ductility and moment redistribution. Transverse reinforcement was provided sufficiently to ensure no shear failure. The concrete with a specified strength of 50 MPa and SD400 bonded reinforcement were used in fabrication of the specimens. Detailed properties of the specimens are shown in Table 1.

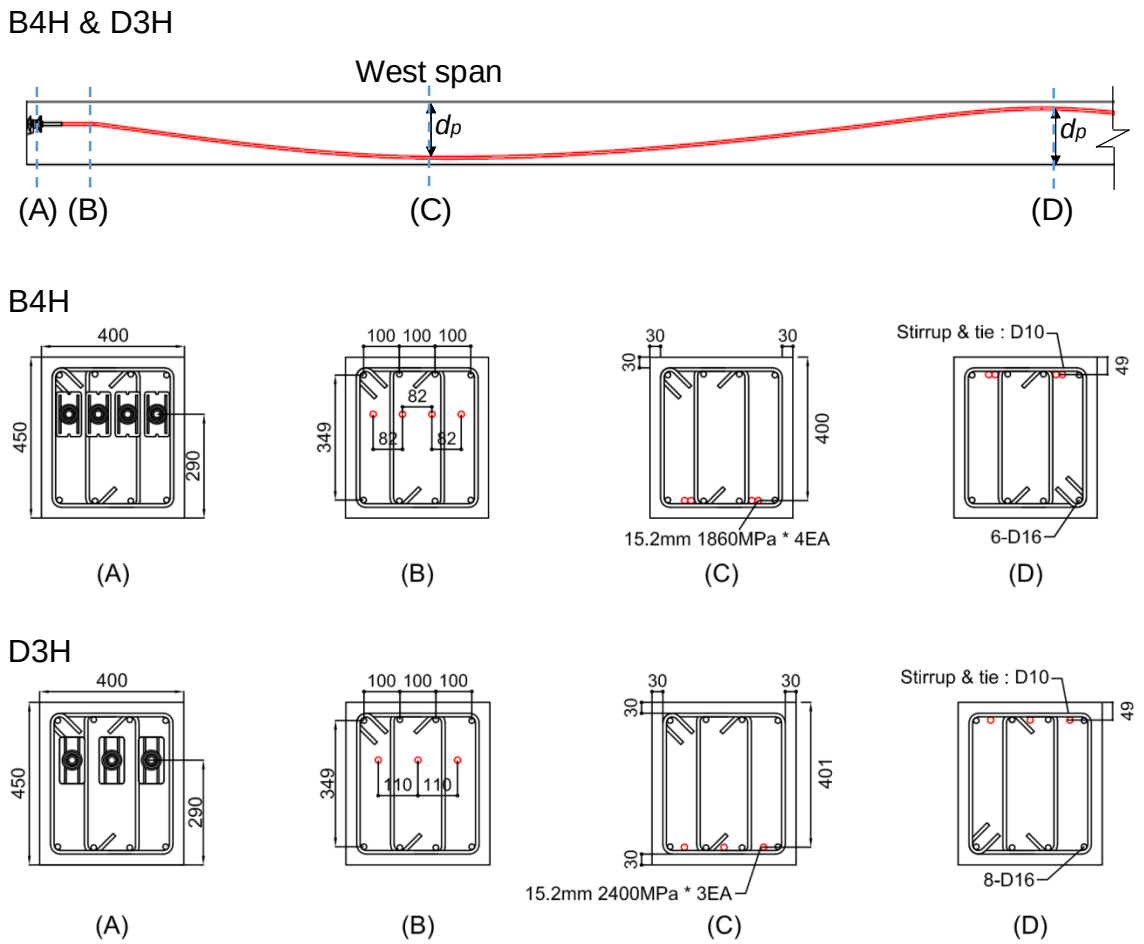


Fig. 1 Geometry of high tendon profile and selected sections of Specimens B4H and D3H (Unit: mm)

In Table 1, effective tendon force is calculated based on the effective tendon stress measured on the jacking end before the testing. The $M_n$ is calculated based on the $f_{ps}$ value in the same table, which is obtained using ACI 318-14 (ACI, 2014) and the effective tendon stress measured on the jacking end before the testing. The geometry of the high tendon profile and configuration of the typical sections are shown in Fig. 1. As shown in the Fig. 1, the tendon profile is symmetric about the centerline. For the specimens with high (B4H and D3H) and low (B4L and D3L) tendon profiles, the distances between the extreme compression fiber to the centroid of the tendon ($d_p$) are 402 mm and 313 mm, respectively. The concrete cover was kept to be 30 mm. Steel of D16 was used for longitudinal reinforcement, and steel of D10 was used for transverse reinforcement including anchorage zone reinforcement.

### *2.2 Test setup*

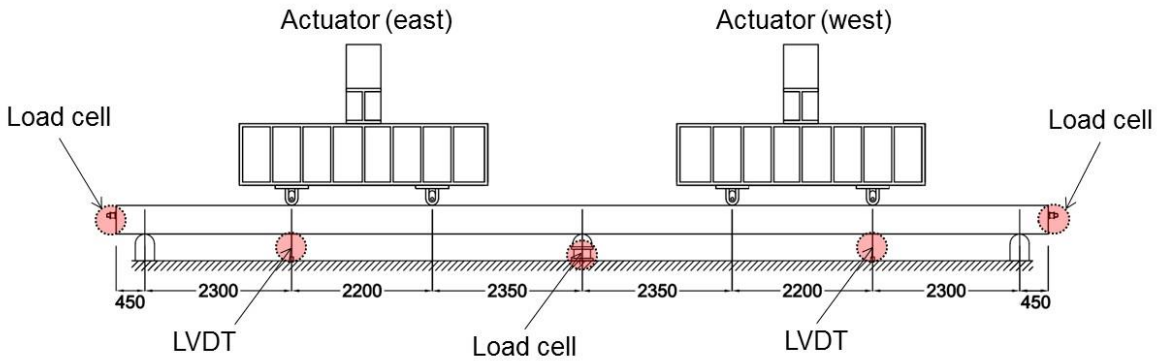


Fig. 2 Two-span beam specimen (B4H) and test set-up elevation view (Unit: mm)

As shown in Fig. 2, four point loads were applied by two actuators. Static load was applied vertically until the strength of the specimen drops by a certain amount. A load cell was placed under the center support to measure the reaction force in real time during the test. The tendon force was measured at the ends of the beam using donut-shaped load cells. Two LVDTs were installed at the locations where the maximum deflections are expected.

## 3. FRICTION LOSS IN POST-TENSIONING TENDONS

In post-tensioning systems, friction force is caused between the strand and surrounding materials, which are either plastic sheathings or steel ducts. The amount of friction can be estimated by using the wobble coefficient ($K$) and coefficient of curvature friction ( ). In this study, using the obtained data from the load cells, tendon stress distributions for the specimens were obtained. This was done assuming that the wobble coefficient and curvature coefficient in the same tendon profile are the same regardless of the strength of strands.

As shown in Fig. 3, the stress profile is triangular shaped due to the stress loss produced by the anchor set behavior at the jacking end as well as the friction loss. These tendon stress profiles were translated by a certain amount in the –y direction (88.8 MPa and 98.6 MPa in the high-strength and the normal-strength, respectively) during the time gap between the point right after anchor set and the point before the testing. This might be due to concrete elastic shortening and creep and drying shrinkage.

As shown in Fig. 3, tendons with the low profile developed higher stress at the fixed end (14.6 m from jacking end) than those with the high profile. This result indicates that the friction loss along the tendon is greater for the larger curvature variation. The high-strength strands developed larger friction loss than that of the normal-strength strands. This was likely because even though the same coefficients were assumed to calculate the friction loss in each tendon profile type, the stress level that the strands were subjected to was different.

Also, the tendon stress at each critical section is presented in Fig. 3. These points were used as $f_{se}$, which is the effective stress of the tendon after subtracting the additional stress loss mentioned previously.

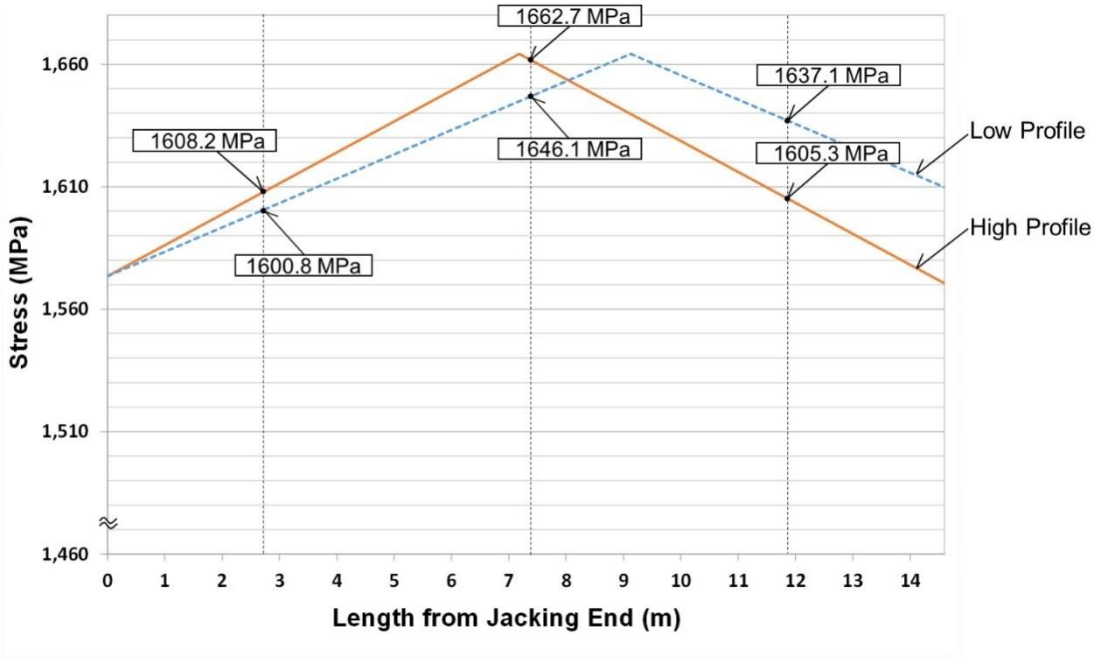


Fig. 3 Generalized high-strength tendon stress profile after anchor set

## 4. Beam Test Results

Four specimens had the two main variables; 1) strand strength and 2) tendon profile. Every specimens except for the B4H specimen B4H showed flexural failure mode at the location very close to the expected critical sections. Fig. 4 shows the typical failure occurred in the D3L specimen. Specimen B4H also showed flexural failure similar to other specimens. However, one of the strands in the B4H specimen fractured at the point of 110 mm displacement. The specimen developed only 70% of its expected strength compared to D3H which was designed to have almost similar strength. The comparison of ultimate flexural strengths between different strand strengths is only possible in the low-profile group; B4L and D3L.

Fig. 5 and Fig. 6 show the load-deflection curve for B4L and D3L specimens. The y-axis indicates the summation of the measured load from two actuators on the east and west sides. The x-axis represents the averaged displacement measured from the both actuators. As shown in Fig. 5 and Fig. 6, both of the specimens showed quite ductile behavior. Given the same material properties and specimen configurations except for the strand strength, B4L and D3L had almost the same flexural capacities of 353.6 kN-m and 353.8 kN-m, respectively, as indicated in Table. 1. The measured load-deflection curve of B4L showed a slightly larger peak load than that of D3L by 6.3%. Specimen B4L also developed its peak point at a displacement of 97.2 mm, which is larger than that of D3L (84.4 mm) when its curve reached the maximum total load point. However, the BL4 specimen had a substantial drop just after reaching the peak, whereas DL3

had a gradual loss in load capacity and exhibited a little degree of hardening. This might be due to the smaller post-yield stiffness of high-strength steel. Further research is needed for better explanation.

In Fig. 5 and Fig. 6, the equivalent total actuator load using $f_{ps(ex)}$ and the equivalent total actuator load using $f_{ps(ACI)}$ are presented as horizontal dotted lines, where $f_{ps(ex)}$ is represented as the tendon stress measured using the load cells at the peak point of the load-deflection curve and $f_{ps(ACI)}$ is the calculated tendon stress based on the measured effective tendon stress before the testing and ACI 318 code equation. For the former, the measured average $f_{ps(ex)}$ along the length is used to predict nominal moments at four critical sections. Then the actuator load is calculated such that the nominal moment value at each critical location is produced. Using the same method, the equivalent total actuator load using $f_{ps(ACI)}$ is also obtained with the exception of using $f_{ps(ACI)}$. The discrepancy between the peak measured and calculated loads may be likely because the strain hardening of mild reinforcing bars is not considered in the calculation. More detailed plastic analysis and 3D finite element analysis are required to analyze the test data.

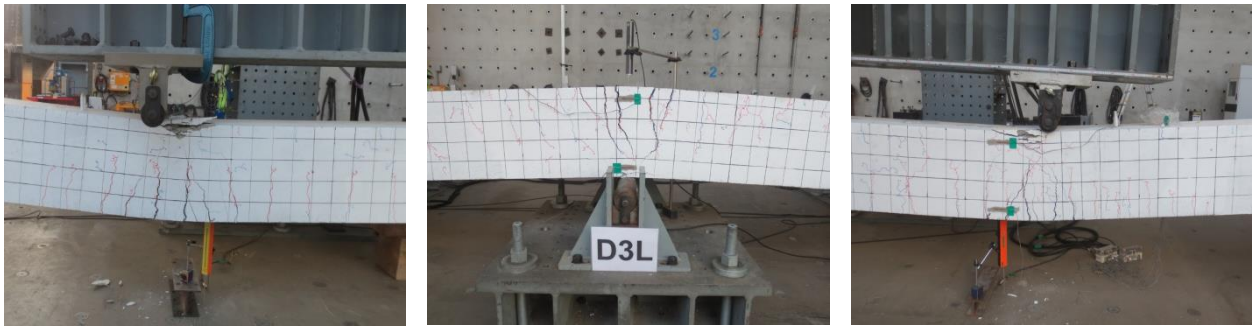


(a) East span (b) Center support (c) West span

Fig. 4 Typical failure mode at each critical section

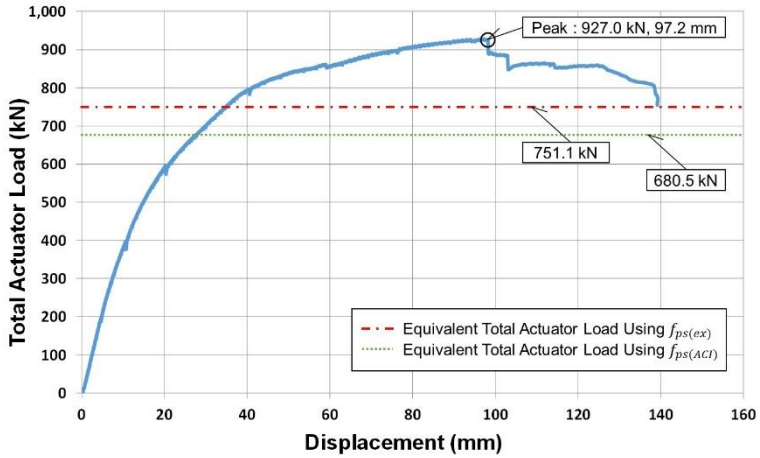


Fig. 5 Load-deflection curve for B4L

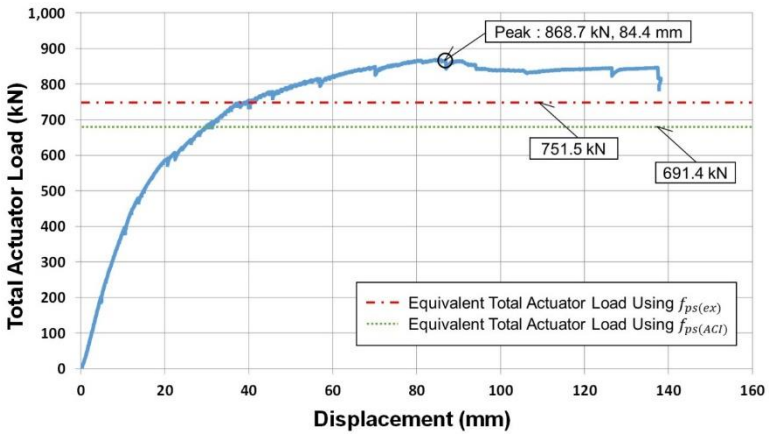


Fig. 6 Load-deflection curve for D3L

## 5. CONCLUSIONS

In this study, four two-span post-tensioned concrete beams were fabricated and tested. The normal-strength and high-strength strands were used for each group of the specimens and their tensile stresses were measured during jacking using the load cells. Based on the obtained data at the fixed and jacking ends, tendon stress profiles were drawn for four different types of tendon profiles and strengths. The beam with high-strength strands (D3L) developed a bit smaller flexural capacity than that of the beam with normal-strength strands only by 6.3%. Further investigation is required for better experimental data assessment.

## REFERENCES

ACI Committee 318 (2014) “Building Code Requirements for Structural Concrete (ACI 318-14) and Commentary,” American Concrete Institute, Farmington Hills, MI, 332.

Yang, J. M., Yim, H. J., Kim, J. K. (2015) "Transfer Length of 2,400 MPa PS Strand in 15 m-long Full-Scale Pretensioned Prestressed Concrete Beam," *Korean Society of Hazard Mitigation,* **15**: 139-146. (in Korean)

Yim, H. J., Kim, J. K., Yang, J. M. (2015), "Experimental Study on the Transfer Length in Pretensioned Prestressed Concrete Beam Using 2,400 MPa PS Strand," *Korean Society of Hazard Mitigation,* **15**: 41-49. (in Korean)